THE JOURNAL OF PHYSICAL CHEMISTRY C

Article

pubs.acs.org/JPCC

Effects of Aromatic Substitution on the Photodimerization Kinetics of *β-trans* Cinnamic Acid Derivatives Studied with ^{13}C Solid-State NMR

Isa Fonseca,[†,#] Maria Baias,[‡,○] Sophia E. Hayes,[§] Chris J. Pickard,[‡] and Marko Bertmer*[,⊥]

[†]Macromolecular Chemistry, Aachen University of Technology, Worringer Weg 1, 52056 Aachen, Germany

[‡]Department of Physics & Astronomy, University College London, Gower Street, QC1E 6BT London, United Kingdom

[§]Department of Chemistry, Washington University, One Brookings Drive, St. Louis, Missouri, 63130, United States

[⊥]Faculty of Physics and Earth Sciences, Leipzig University, Linnéstr. 5, 04103 Leipzig, Germany

Supporting Information

ABSTRACT: In our efforts to study photodimerizations in the solid state, we present data on the influence of the position of aromatic substitution by bromine on the photodimerization rate in cinnamic acid derivatives. Results were obtained by ^{13}C CPMAS NMR spectroscopy together with chemical shift tensor analysis, DFT calculations using the NMR-CASTEP program, and crystal structure data. Reaction rates are highest for *para* bromo substitution, whose parent crystal structure was solved in this work. To explain the differences in photoreaction rate, several factors such as distance between double bonds, best π-orbital overlap of the reacting C═C double bonds, and CSA tensor analysis (using 2D PASS) were taken into account. Calculations of ^{13}C chemical shifts and chemical shift anisotropy tensor parameters show very good agreement with experimental data, including the carboxylic carbon that is hydrogen bonded to the neighboring cinnamic acid molecule. For the cinnamic acid photodimerization, the best angle between reacting double bonds and the smallest degree of molecular reorientation favor faster photoreaction.

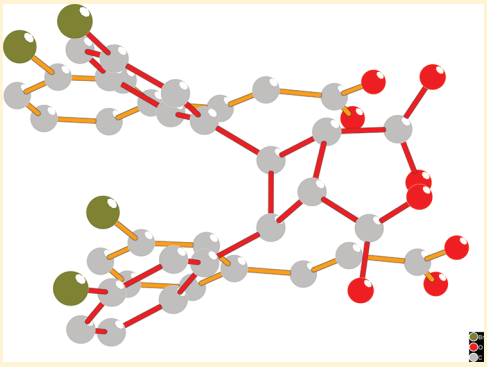

1. INTRODUCTION

Photodimerizations in the solid state can produce highly stereospecific products with high yields, since the relative molecular orientation is fixed in the crystal lattice.[1,2] Furthermore, such molecules that undergo photodimerizations, if they are reversible with light of different wavelengths, can potentially be used as molecular memory or switches and can be envisioned for elements in devices related to miniaturization in the information technology area.[3,4] The [2 + 2] photodimerization between two double bonds to form a cyclobutane ring-like moiety is a model system for such molecular memory structures.[5]

To date, we have studied a series of solid-state photoreactions of cinnamic acid and its derivatives. These studies include differences between the α (head-to-tail arrangement of reacting cinnamic acid molecules)[6,7] and β (head-to-head arrangement)[8] polymorphs of unsubstituted *trans* cinnamic acid and the size effect of substituents, *ortho* methoxy and ethoxy *trans* cinnamic acid.[9] Hereafter, the "*trans*" label will be dropped for simplicity. ^{13}C NMR has been shown to be highly effective for studying the photoreaction because of the large difference in chemical shifts of the reactant (sp^2) olefinic carbons that transform to cyclobutane (sp^3) carbons in the product. Our recent ^{13}C CPMAS studies have demonstrated that unsubstituted α cinnamic acid—existing with a planar cyclobutane ring at the beginning of the reaction but then transforming to a puckered four-membered ring[7]—photoreacts considerably faster than β cinnamic acid[8] because of a shorter distance between double bonds and the smaller reorientations in the molecule necessary for photodimerization in the former. In the *ortho*-substituted cinnamic acids, a direct relation between the angle χ between reacting double bonds and the photoreaction rate was observed, with those closest to 90° reacting fastest.[9] The definition of the angle χ is given in Figure 1. Finally, single-crystal ^{13}C NMR of the photodimerization of α cinnamic acid has been used to identify the degree of disorder in the single-crystal to single-crystal transformation.[10]

Herein, we report on the influence of the position of aromatic substitution on the photoreaction rate. For this, bromo-substituted cinnamic acids were chosen because they are readily available in the *ortho*, *meta*, and *para* forms, and all crystallize in the head-to-head β polymorph. Together with ^{13}C CPMAS spectra, we also determine the chemical shift anisotropy tensors that can indicate reorientations of the molecule between reactant and product structure. For the calculation of NMR parameters, information from published crystal structures (including the one for *para* bromo *trans*

Received: February 21, 2012
Revised: May 8, 2012
Published: May 14, 2012

dx.doi.org/10.1021/jp301703d | J. Phys. Chem. C 2012, 116, 12212−12218

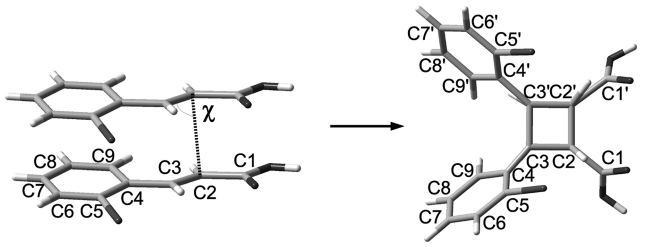

β-*o*-bromo cinnamic acid β-*o*-bromo truxinic acid

Figure 1. Reaction scheme shown for *β-ortho* bromo cinnamic acid reacting to the corresponding truxinic acid. Uniform carbon numbering is used for all samples, with the Br atom connected to carbons C6 and C7 for the *meta* and *para* position, respectively. The angle χ indicates the angle between reacting double bonds used later in the text.

cinnamic acid solved in this publication) is used as input for the NMR-CASTEP code.[11]

The first studies on β bromo cinnamic acid date back to 1886.[12] More recent work investigated the polymorphic phase transformation from the γ to the more stable β modification of *meta* bromo cinnamic acid at temperatures above 100 °C monitored by X-ray powder diffraction.[13] Recently, IR studies characterized—among others—the photodimerization of single-crystalline *para* bromo cinnamic acids.[14] Interestingly, from theoretical predictions on *para* bromo cinnamic acid,[15] it should be impossible that the photoreaction conversion reaches 100%, which is in contrast to our findings here.

2. EXPERIMENTAL SECTION

Commercial *ortho*, *meta*, and *para* bromo cinnamic acids (Aldrich, 95, 98, and 98% purity, respectively) were used for the crystallization of the corresponding β-polymorphs. The *ortho* and *para* derivatives were crystallized from a hot solution of diluted ethanol (ethanol and water) and the *meta* derivative from a hot solution of 99% acetic acid.[16] The different derivatives exhibit different crystal shapes and sizes. The *ortho* bromo cinnamic acid crystallizes in colorless thin laths. A sample of 1−2 mm crystals was selected using mesh sieves. However, due to the large aspect ratio of the crystals (thin laths), there is still a distribution of crystal sizes. The *meta* bromo cinnamic acid crystallizes in semitransparent cubic crystals, which were also selected in the 1−2 mm size range. Finally, the *para* bromo cinnamic acid crystallizes in small white needles with sizes of less than 500 μm, which did not require sieving. Crystallization of the *para* derivative for X-ray diffraction was accomplished via slow evaporation from a methanol−water solution. The preparation of the corresponding photoproducts, bromo truxinic acids, was carried out under broad-band UV irradiation using an OSRAM Ultravitalux water-cooled arc lamp for consecutive irradiation periods of 10 min, with agitation of the powders between each consecutive period. The reaction product, *ortho* bromo truxinic acid, was separated from cinnamic acid by selective dissolution in ether, while the *meta* and *para* truxinic acids were separated from the reactant using toluene, the reaction products being the insoluble fraction in all three cases.[16] The photoproduct samples were then evacuated for several days to extract any remaining solvent.

For monitoring the kinetics, a different photoirradiation procedure was used (for details, see ref 8). Individual samples were irradiated continuously for the total time given (see below), rather than sequential irradiation of a single sample with spectra recorded in between. This procedure was followed to prevent the loss of crystallinity from packing and unpacking of the MAS rotor between the photoirradiation periods.

NMR experiments were performed on a Bruker Avance DSX 500 spectrometer (unless specified otherwise) with frequencies of 500.46 and 125.84 MHz for ^{1}H and ^{13}C, respectively. For the kinetics studies, a spinning frequency of 6.5−8 kHz was chosen to avoid overlap of signals with spinning sidebands. The recycle delays of the respective cinnamic acids before irradiation were 1200 s for the *ortho*, 600 s for the *meta*, and 1000 s for the *para* bromo samples, as determined from ^{1}H MAS measurements. The ^{1}H $\pi/2$ pulse length was 2.5 μs and the contact time 1 ms. Some of the dipolar dephasing[17] spectra, where the ^{1}H deoupling was turned off for a certain time, were recorded on a Bruker Avance 400 spectrometer with frequencies of 400.13 and 100.62 MHz for ^{1}H and ^{13}C, respectively, with similar measurement parameters. The chemical shift anisotropy tensor studies were executed using the 2D PASS[18] pulse sequence, the modified version with five π-pulses.[19,20] Measurements were made at a spinning frequency of 1.5 kHz, in order to have a number of spinning sidebands to improve the accuracy of the analysis, using the Herzfeld−Berger method[21] with the HBA software package.[22] All the spectra were referenced to TMS using glycine as a secondary reference.

The crystal structure of *para* bromo cinnamic acid was solved via powder X-ray diffraction in this work, and the crystal parameters were deposited at the Cambridge Crystallography Data Centre (CCDC #801089).

NMR theoretical calculations were performed using the CASTEP software package.[11] In the simulations, the atom positions were taken from the X-ray crystal structures for *ortho*[14] and *meta* cinnamic acid[23] as well as for *meta* bromo truxinic acid.[24] For *para* bromo cinnamic acid, the crystal structure was solved within this work (see above) and used for the simulations.

DFT calculations have been shown to yield good ^{13}C chemical shift predictions, as we have demonstrated previously.[8,9] However, an isolated molecule was the basis for these calculations such that the influence of hydrogen bonds between carboxylic acid groups like those found in cinnamic acid derivatives was not accounted for. Since these hydrogen bonds have strong structure-directing effects, the calculated chemical shift of the carboxylic carbon was less accurate, with differences between calculation and experiment of up to 10 ppm. For chemical moieties like these, the NMR-CASTEP code[11] yields better agreement, as it calculates chemical shieldings using periodic boundary conditions. The calculations of NMR parameters in solids using the NMR-CASTEP code rely on density functional theory and make use of plane waves together with pseudopotentials in a gauge-including projector-augmented wave (GIPAW) approach.[25] Since this method implies the use of periodic boundary conditions to describe the translational symmetry of a solid, this approach is suitable for modeling the response of nuclei in a crystal exposed to an applied external magnetic field. GIPAW methods have been successfully applied to calculate NMR parameters such as shielding tensors,[26] quadrupolar couplings,[27,28] electric field gradients,[29] or *J*-couplings[30] in various chemical systems.

A geometry optimization was performed on all the cinnamic acid crystal structures obtained from the crystallographic database by fixing the unit cell and all the heavy atoms and relaxing only the proton positions. The geometry optimizations

were done with a cutoff energy of 800 eV using the GGA (BPE)[31] exchange correlation functional, with integrals taken over the Brillouin zone by using a Monkhorst–Pack grid of minimum sample spacing of 0.03 $Å^{-1}$. After optimization, the average residual forces on atoms were up to a maximum of 0.366 eV/Å on the C atoms and 0.003 eV/Å on the H atoms for the *ortho* bromo cinnamic acid, 0.306 eV/Å on C and 0.013 eV/Å on H for *meta* bromo cinnamic acid, 0.365 eV/Å on C and 0.004 eV/Å for H for *para* bromo cinnamic acid, and 0.215 eV/Å on C and 0.001 eV/Å on H for *meta* bromo truxinic acid. On the relaxed structures, the NMR parameters were calculated using the GGA (PBE)[31] exchange correlation functional. We used a cutoff energy of 800 eV for the calculation of NMR parameters and performed the integration over the Brillouin zone using an MP grid of 0.03 $Å^{-1}$. The CASTEP calculated chemical shieldings σ_{calc} were converted into calculated chemical shifts δ_{calc} using the relation $\delta_{calc} = \sigma_{ref} - \sigma_{calc}$, with the value of σ_{ref} obtained as an internal reference for each structure, determined by a linear regression between calculated and experimental shifts.

3. RESULTS AND DISCUSSION

3.1. ^{13}C Spectra. The photodimerization reaction is illustrated schematically in Figure 1 for the example of *ortho* bromo cinnamic/truxinic acid, showing the β head-to-head packing in the crystal. Photodimerization then leads to the corresponding β-truxinic acid. ^{13}C CPMAS spectra of the three cinnamic acid derivatives are summarized in Figure 2 with indications of the results from CASTEP calculations plotted below each individual spectrum. The assignments of each carbon atom are given in the Supporting Information. The three spectra are quite similar, as expected. Signals of carboxylic and olefinic carbons have almost identical chemical shifts among the three samples, with only the one olefinic carbon signal of the *ortho* sample at 117 ppm being slightly shifted to higher frequency. Aromatic carbon signals are grouped around 130 ppm, and show differences between samples due to the effect of bromine being at different positions on the aromatic ring. It is worth noting the line width of the aromatic carbon signals is smaller in the case of the *meta* bromo cinnamic acid, indicating greater long-range order.

The very good agreement between experimental and calculated spectra is evidenced by the small root-mean-square deviation values obtained from the comparison of experimental chemical shifts and the CASTEP calculated values. Good rmsd values are obtained for all cinnamic acid derivatives, and they are provided in the Supporting Information for each structure. For the rmsd value, the carbon next to bromine was excluded, since the calculation results yield a systematic error for this carbon. Further details on the assignments and dipolar dephasing experiments[17] can be found in the Supporting Information. We remark that NMR signals from the carbon atoms next to the bromine atom cannot be resolved experimentally (see also the discussion below).

For the photoproducts, Figure 3 shows the three ^{13}C CPMAS spectra together with the simulation for *meta* bromo truxinic acid. Assignments of individual carbon atoms are given in the Supporting Information. For the photoproducts, the carbon atom next to bromine is visible in the dipolar dephasing spectra (Figure 4), seen as a broad, featureless line (along with

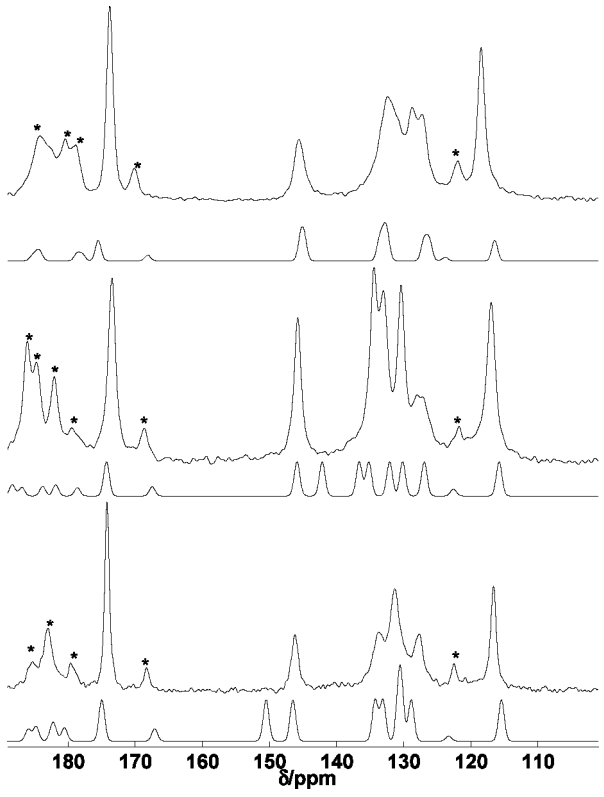

Figure 2. ^{13}C CPMAS spectra of *ortho*, *meta*, and *para* bromo cinnamic acid (from top to bottom). Asterisks mark spinning sidebands. Below each spectrum are the results from CASTEP calculations.

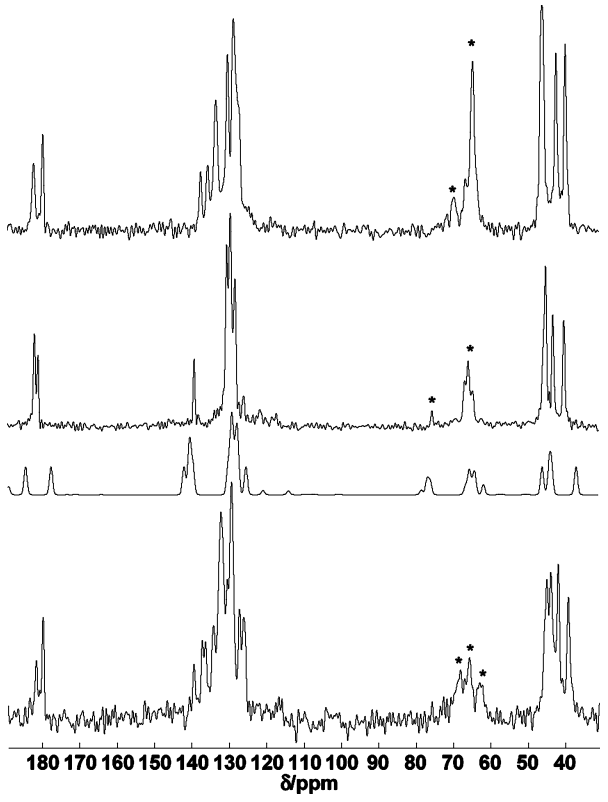

Figure 3. ^{13}C CPMAS spectra and *ortho*, *meta*, and *para* bromo truxinic acids (from top to bottom). Asterisks mark spinning sidebands. For *meta* truxinic acid, the simulated spectrum is given below the corresponding spectrum.

dx.doi.org/10.1021/jp301703d | J. Phys. Chem. C 2012, 116, 12212–12218

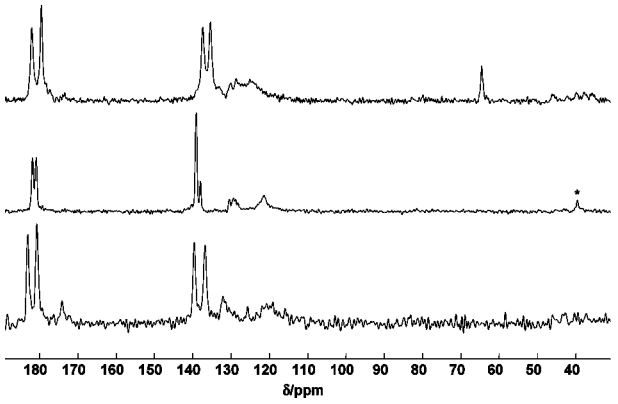

Figure 4. ^{13}C CPMAS dipolar dephasing spectra of *ortho*, *meta*, and *para* bromo truxinic acids (from top to bottom). The signal at 65 ppm for *ortho* bromo truxinic acid is due to remaining solvent. The asterisk denotes a spinning sideband.

signals for the ipso-carbon and the carboxyl carbon). Individually resolved resonances, similar to those seen in refs 32−34, are not observed here, possibly due to large quadrupolar couplings and overlap between ^{79}Br and ^{81}Br coupled signals.

For all samples, three to four cyclobutane carbon signals are present in the 40−50 ppm range, indicating nonsymmetric carbon positions. This finding suggests that the cyclobutane ring is nonplanar, as was observed in the case of α truxillic acid.[6] The existence of two signals each for the carboxylic and ipso carbons is further evidence of the lack of inversion symmetry (and, hence, lack of planarity).

3.2. Photoreaction Kinetics and Influence of Substituent Position. For studying the photoreaction kinetics of the β bromo cinnamic acids, samples were irradiated and the corresponding ^{13}C CPMAS spectra obtained as a function of total light irradiation time. For *para* bromo cinnamic/truxinic acid, such a series of spectra is shown in Figure 5. The corresponding stack plots of the other two systems can be found in the Supporting Information.

The resulting kinetics curves for *ortho*, *meta*, and *para* bromo cinnamic acid are depicted in Figure 6. For comparison, the kinetics curve of unsubstituted β *trans* cinnamic acid[8] is shown as well.

The kinetics curves are fit to the JMAK (Johnson, Mehl, Avrami, Kolmogorov) model for nucleation and growth[35−39] using the equation

$$X(t) = 1 - e^{-kt^n} \quad (1)$$

in a manner similar to its application for broadband irradiation in cinnamic acid demonstrated previously.[6]

Herein, $X(t)$ describes the transformed fraction, k the reaction rate, and n (the Avrami exponent) the dimensionality of the growth and progression of photoreaction. The latter takes values of 2, 3, and 4 for one-, two-, and three-dimensional growth, respectively, in the case that "seeds" (or "nuclei") are formed during the reaction. Here, all the curves fit very well with a value for n very close to 1 and therefore are indistinguishable from a first-order kinetics curve. A value of the Avrami exponent close to 1 is indicative of product homogeneity throughout the crystal (implying thorough light penetration).

The extracted parameters are summarized in Table 1. It can be seen that for all three samples n is smaller but rather close to

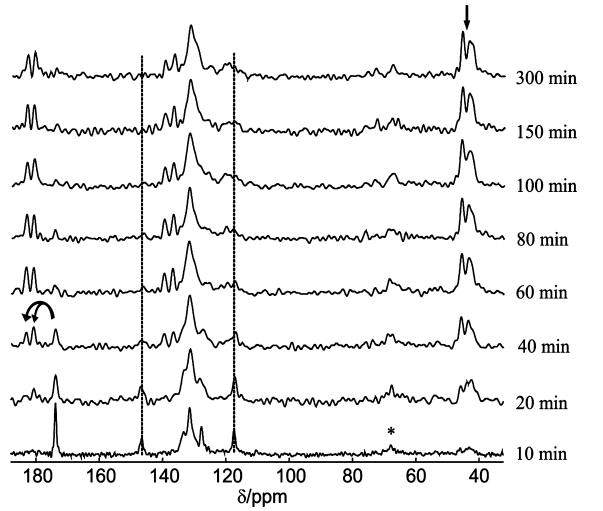

Figure 5. Stack plot of ^{13}C CPMAS spectra of irradiated *para* bromo cinnamic acid as a function of total photoirradiation time. The dashed lines mark the vinyl positions, the curved arrows mark the shift from one to two carboxyl signals upon photoreaction, and the straight arrow indicates the cyclobutane peaks. To avoid confusion, spinning sidebands are marked with an asterisk only for the bottom spectrum.

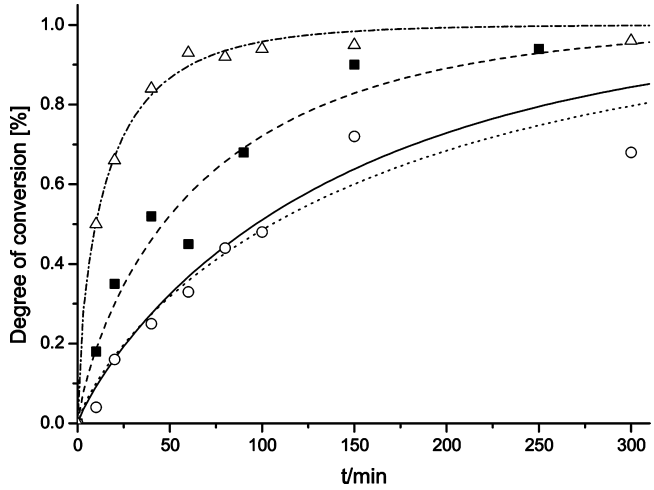

Figure 6. Photodimerization kinetics curves of *ortho* (dashed line, solid squares), *meta* (dotted line, open circles), and *para* bromo cinnamic acid (dash-dotted line, open triangles) together with that of unsubstituted β cinnamic acid (solid line). The fit functions according to the JMAK model are given by lines.

1. By comparison, α *trans* cinnamic acid had an Avrami exponent of approximately 1.7.

Since n is almost the same for all four samples, the growth of the product phase is approximately the same for all. Then, the reaction rate can be directly compared, showing that k for *meta* bromo cinnamic is about the same as that for unsubstituted β

Table 1. Parameters of the JMAK Equation for the Different Cinnamic Acids

type of cinnamic acid	n	k (min^{-1})
ortho bromo	0.79 ± 0.11	0.033 ± 0.002
meta bromo	0.80 ± 0.13	0.017 ± 0.001
para bromo	0.69 ± 0.03	0.156 ± 0.002
unsubstituted β	0.87 ± 0.11	0.013 ± 0.001

dx.doi.org/10.1021/jp301703d | J. Phys. Chem. C 2012, 116, 12212−12218

cinnamic acid, while that of *ortho* bromo cinnamic acid is twice as large and that of *para* bromo cinnamic acid is more than 9 times larger.

To find an origin for these differences, we have examined several possible sources. At first, the UV absorption spectra show only minor differences between the different cinnamic acids (see the Supporting Information) such that differences in electronic states excited by UV radiation can be excluded as the source of different reaction rates.

The chemical shift anisotropy (CSA) tensor is sensitive to the electron density and orientation at the site of each carbon atom. Reorientations between reactant and product molecules together with atomic movement have to occur for the [2 + 2] cycloaddition reaction to take place and form the photodimer. This effect is illustrated in Figure 7 by a superposition of the

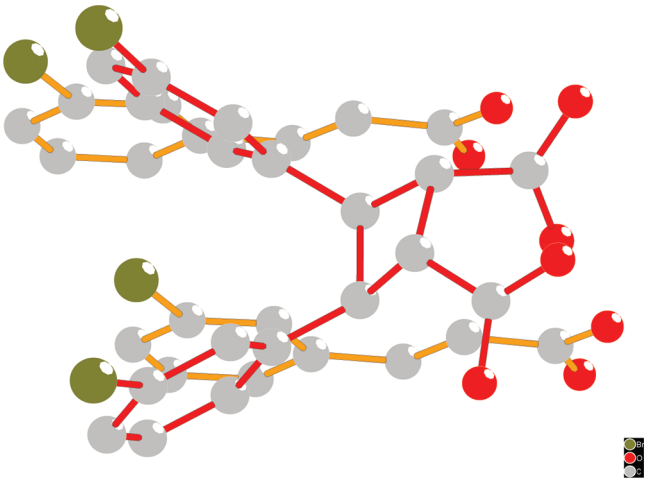

Figure 7. Superposition of reactant and product molecules in the photodimerization of *meta* bromo cinnamic acid to indicate reorientational changes due to reaction. The representations are taken from the crystal structures.[23,24] Atoms connected by yellow bonds indicate the two reactant molecules, those connected by red bonds indicate the product molecule.

two reacting *meta* bromo cinnamic acid molecules and the resulting *meta* bromo truxinic acid molecule as obtained from the crystal structures. These local relative geometric rearrangements can affect the local electronic structure and with that the chemical shift anisotropy.

In a system with many carbons, separation of the CSA tensor of each carbon is necessary. One method to accomplish this is the 2D PASS approach at low spinning speeds[18−20] which separates spinning sidebands by their order in the second dimension of a spectrum. From the set of individual spinning sidebands of each carbon atom, the corresponding CSA tensor elements can be obtained, e.g., using the Herzfeld−Berger analysis method[21] with the HBA program.[22] As an example, Figure 8 illustrates the 2D PASS spectrum of *ortho* bromo cinnamic acid with resolved spinning sidebands up to 7th order in both directions. The full set of 2D PASS spectra, and the resulting tables with CSA tensor values, including the results from CASTEP calculations, are summarized in the Supporting Information.

We use differences in principle values of the tensors (δ_{11}, δ_{22}, δ_{33}) between truxinic and cinnamic acids as reporters of structural change. In other words, large differences in these values can be connected to movement of sites as a consequence

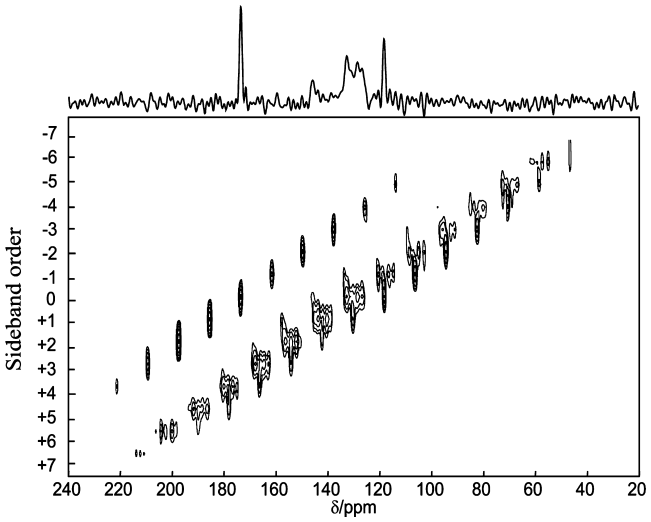

Figure 8. ^{13}C 2D PASS NMR of *ortho* bromo cinnamic acid.

of the [2 + 2] photocycloaddition. Figure 9 summarizes the results of the CSA tensor analysis for the three different bromo-substituted systems. The data are illustrated in a way that the differences between the tensor parameters from truxinic and cinnamic acid for the individual carbon atoms are plotted. A large deviation from the horizontal line through the origin indicates a large change to the principal value. Only the five aromatic carbons excluding the ipso-carbon are shown. The remaining carbons experience large shifts from the change of hybridization upon reaction (C2 and C3) or by being directly adjacent to them (C1 and C4). For the *ortho* and *para* system, the carbon atom next to bromine is excluded, since it is not well resolved in the parent (cinnamic acid) spectra. All plots have the same scaling to better illustrate the differences between the different samples.

Comparing the three plots, the smallest deviation is seen for the *ortho* system, indicating that only small changes to the principal tensor values are necessary between reactant and product. Only carbon C8 shows a significant deviation. For the *para* system, the changes are larger overall, and, with the exception of C9, are in the range +10 to −15 ppm. The largest changes are observed for the *meta* system for several carbon atoms, indicating that significant reorientations occur upon reaction. The results for the *meta* system, meaning large structural rearrangement, fit with our observations that the photodimerization rate is the slowest for this system.

Additional information can be taken from the available crystal structures, i.e., both the distance between reacting double bonds and the angle between them. In our previous investigation of the *ortho* substituted α-cinnamic acids, the distance between double bonds did not correlate with the photodimerization rate but the system with the angle χ between double bonds being closest to 90° showed the fastest reaction because it affords the best π-orbital overlap.[9] The corresponding parameters for the bromo-substituted systems are summarized in Table 2.

The distances between the reacting double bonds are relatively similar with the *para* compound being the smallest and the unsubstituted β cinnamic acid the largest. However, the angles between the double bonds are all different from 90°, which is best for π-overlap, since then the double bonds are aligned with the values for *meta* and *para* bromo cinnamic acid being closest to the optimum value.

dx.doi.org/10.1021/jp301703d | J. Phys. Chem. C 2012, 116, 12212−12218

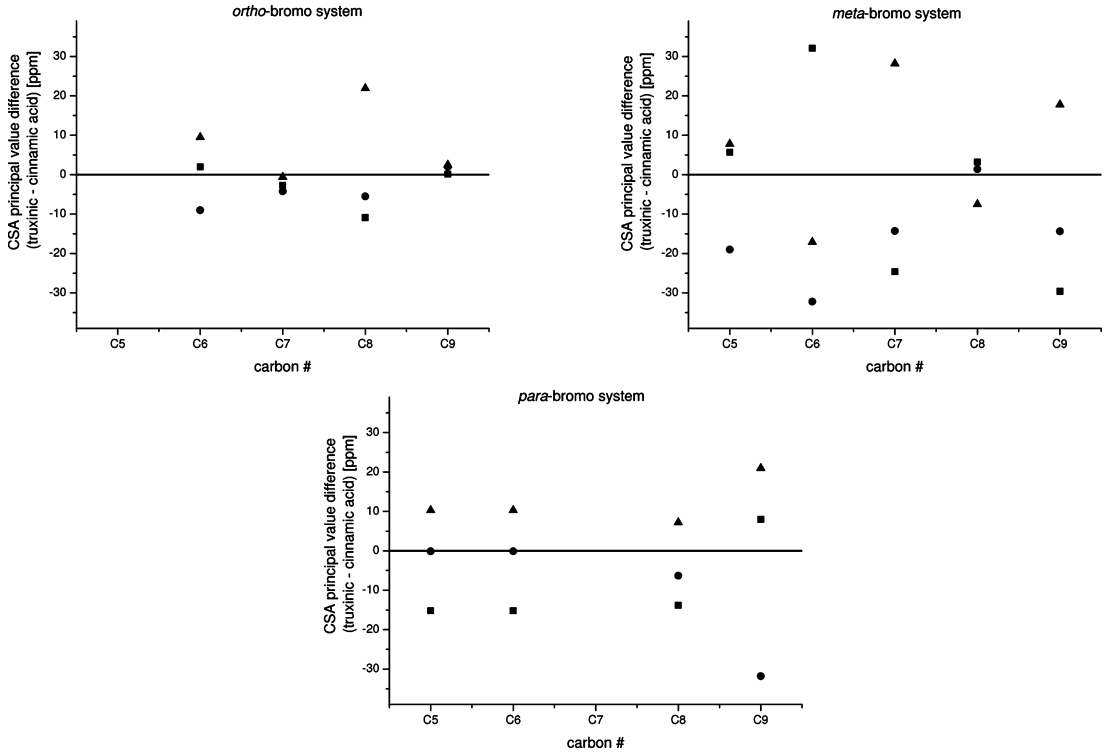

Figure 9. Differences in CSA principal values δ_{11} (squares), δ_{22} (circles), and δ_{33} (triangles) before and after photoreaction for the *ortho* (top left), *meta* (top right), and *para* (bottom) bromo system.

Table 2. Distance and Angle between Reacting Double Bonds and Corresponding References for the Crystal Structures

type of cinnamic acid	distance (pm)	angle χ (deg)	reference
ortho bromo	396.8	67.36	14
meta bromo	398.8	76.46	23
para bromo	390.43	76.91	this contribution
unsubstituted β	401.52	81.827	40

Combining all the information, the differences in reaction rate seem to be the result of an interplay of several parameters. *Para* bromo cinnamic acid, being the one with the fastest observed reaction rate, has the most optimal angle between double bonds, and shows only small atomic reorientations (CSA changes) during the reactions. Compared to this, the slower-reacting *ortho* bromo cinnamic acid has similar values for the reorientations, and the angle between double bonds is worse. For the *meta* bromo cinnamic acid, though the angle between double bonds is similar to the *para* system, the largest reorientations are found as shown by the tensor analysis. The need for substantial molecular movement for reaction slows down the reaction rate, as has been observed in earlier studies,[8] leading overall to the slowest reaction rate for the different aromatic substituted systems.

Therefore, in the bromine substituted cinnamic acids studied here, only a combined analysis of CSA principal tensor values and relative angle between reacting double bonds can explain the differences in the observed photoreaction rates.

4. CONCLUSIONS

The characterization of three β *trans* bromo cinnamic acid derivatives, as well as their photoproducts, was successfully carried out using ^{13}C solid-state NMR with the support of theoretical calculations. The latter show excellent agreement for all carbons including the carboxyl carbon due to the incorporation of periodic boundary conditions to account for hydrogen bonding in the NMR CASTEP routine. The photoreaction kinetics of the three derivatives was analyzed on the basis of the JMAK model, where for all three cases the nucleation and growth appears to be homogeneous throughout the crystal. The photoreaction rate was observed to be the largest for *para* and the smallest for *meta* substituted species. Explanations for this dependence can be taken from the comparative CSA tensor analysis of the three derivatives before and after photoreaction as well as the angles between the reacting double bonds. The distance between double bonds does not appear to be a major driver in the systems studied, since the values are all comparable.

The information gathered in this contribution shows that aromatic substitution clearly influences the photoreaction of β cinnamic acids, which becomes more favorable for *para* substitution. Summarizing our results together with our previous publications,[6,8,9] we observed that the α orientation (head-to-tail) has a faster reaction rate than the β orientation (head-to-head) independent of substitution (for the range of samples studied). Larger substituents and substitution in *para* (or *ortho*) positions seem to increase the reaction rate. Other influences on the reaction rate include the relative angle between the reacting double bonds.

On the basis of these results, we want to extend our studies on photodimerization kinetics toward cinnamic acid derivatives as side chains in polymers[41,42] or embedded in layered double hydroxides (LDH)[43,44] to progress in the direction of materials with potential applications as optical memory.

dx.doi.org/10.1021/jp301703d | J. Phys. Chem. C 2012, 116, 12212−12218

■ ASSOCIATED CONTENT

Supporting Information

Experimental and theoretical chemical shifts of all compounds, stack plots of photoreaction kinetics, UV−vis spectra, 2D PASS spectra, and experimental and theoretical CSA parameters. This material is available free of charge via the Internet at http://pubs.acs.org.

■ AUTHOR INFORMATION

Corresponding Author

*E-mail: bertmer@physik.uni-leipzig.de.

Present Addresses

[#]BASF SE, Carl-Bosch-Strasse 38, 67056 Ludwigshafen, Germany.

[○]Universitè de Lyon, Centre de RMN à Très Hauts Champs, CNRS/ENS Lyon/UCBL, 5 Rue de la Doua, 69100 Villeurbanne, France.

Notes

The authors declare no competing financial interest.

■ ACKNOWLEDGMENTS

We thank the group of Prof. Dr. Harald Krautscheid from the Chemistry Department at Leipzig University, especially Jörg Lincke and Daniel Lässig, for solving the crystal structure of *para* bromo cinnamic acid via X-ray diffraction. M.B. thanks the German research foundation (DFG) for supporting this work (BE 2434/2-2).

■ REFERENCES

(1) Feldman, K. S.; Campbell, R. F. *J. Org. Chem.* **1995**, *60*, 1924−1925.

(2) MacGillivray, L. R.; Reid, J. L.; Ripmeester, J. A. *J. Am. Chem. Soc.* **2000**, *122*, 7817−7818.

(3) Feringa, B. L.; Jager, W. F.; de Lange, B. *Tetrahedron* **1993**, *49*, 8267−310.

(4) Dvornikov, A. S.; Liang, Y.; Cruse, C. S.; Rentzepis, P. M. *J. Phys. Chem. B* **2004**, *108*, 8642−8658.

(5) Feringa, B. L.; van Delden, R. A.; Koumura, N.; Geertsema, E. M. *Chem. Rev.* **2000**, *100*, 1789−1816.

(6) Bertmer, M.; Barnes, A. B.; Nieuwendaal, R. C.; Hayes, S. E. *J. Phys. Chem. B* **2006**, *110*, 6270−6273.

(7) Nieuwendaal, R. C.; Bertmer, M.; Hayes, S. E. *J. Phys. Chem. B* **2008**, *112*, 12920−12926.

(8) Fonseca, I.; Hayes, S. E.; Blümich, B.; Bertmer, M. *Phys. Chem. Chem. Phys.* **2008**, *10*, 5898−5907.

(9) Fonseca, I.; Hayes, S. E.; Bertmer, M. *Phys. Chem. Chem. Phys.* **2009**, *11*, 10211−10218.

(10) Nieuwendaal, R. C.; Mattler, S. J.; Bertmer, M.; Hayes, S. E. *J. Phys. Chem. B* **2011**, *115*, 5785−5793.

(11) Segall, M. D.; Lindan, P. J. D.; Probert, M. J.; Pickard, C. J.; Hasnip, P. J.; Clark, S. J.; Payne, M. C. *J. Phys.: Condens. Matter* **2002**, *14*, 2717−2744.

(12) Sudborough, J. J.; Thompson, K. J. *J. Chem. Soc., Trans.* **1903**, *83*, 1153−1167.

(13) Ahn, S.; Harris, K. D. M.; Kariuki, B. M.; Zin, D. M. S. *J. Solid State Chem.* **2001**, *156*, 10−15.

(14) Jenkins, S. L.; Almond, M. J.; Atkinson, S. D. M.; Drew, M. G. B.; Hollins, P.; Mortimore, J. L.; Tobin, M. J. *J. Mol. Struct.* **2006**, *786*, 220−226.

(15) Savion, Z.; Wernick, D. L. *J. Org. Chem.* **1993**, *58*, 2424−2427.

(16) Cohen, M. D.; Schmidt, G. M. J.; Sonntag, F. I. *J. Chem. Soc.* **1964**, 2000−2013.

(17) Opella, S. J.; Frey, M. H. *J. Am. Chem. Soc.* **1979**, *101*, 5854−5856.

(18) Dixon, W. T. *J. Chem. Phys.* **1982**, *77*, 1800−1809.

(19) Antzutkin, O. N.; Shekar, S. C.; Levitt, M. H. *J. Magn. Reson., Ser. A* **1995**, *115*, 7−19.

(20) Ivchenko, N.; Hughes, C. E.; Levitt, M. H. *J. Magn. Reson.* **2003**, *164*, 286−293.

(21) Herzfeld, J.; Berger, A. E. *J. Chem. Phys.* **1980**, *73*, 6021−30.

(22) Eichele, K.; Wasylishen, R. E. *HBA*, version 1.6.12; Dalhousie University and Universität Tübingen, 2010.

(23) Kanao, S.; Kashino, S.; Haisa, M. *Acta Crystallogr., Sect. C* **1990**, *46*, 2436−2438.

(24) Kanao, S.; Kashino, S.; Haisa, M. *Acta Crystallogr., Sect. C* **1990**, *46*, 2439−2442.

(25) Pickard, C. J.; Mauri, F. *Phys. Rev. B* **2001**, *63*, 245101.

(26) Harris, R. K.; Hodgkinson, P.; Pickard, C. J.; Yates, J. R.; Zorin, V. *Magn. Reson. Chem.* **2007**, *45*, S174−S186.

(27) Ashbrook, S. E.; Pollés, L. L.; Gautier, R.; Pickard, C. J.; Walton, R. I. *Phys. Chem. Chem. Phys.* **2006**, *8*, 3423−3431.

(28) Ashbrook, S. E.; Pollès, L. L.; Pickard, C. J.; Berry, A. J.; Wimperis, S.; Farnan, I. *Phys. Chem. Chem. Phys.* **2007**, *9*, 1587−1598.

(29) Yates, J. R.; Pickard, C. J.; Payne, M. C.; Dupree, R.; Profeta, M.; Mauri, F. *J. Phys. Chem. A* **2004**, *108*, 6032−6037.

(30) Joyce, S. A.; Yates, J. R.; Pickard, C. J.; Brown, S. P. *J. Am. Chem. Soc.* **2008**, *130*, 12663−12670.

(31) Perdew, J. P.; Burker, K.; Ernzerhof, M. *Phys. Rev. Lett.* **1996**, *77*, 3865−3868.

(32) Aliev, A. E.; Harris, K. D. M.; Barrie, P. J.; Camus, S. *J. Chem. Soc., Faraday Trans.* **1994**, *90* (24), 3729−3730.

(33) Aliev, A. E.; Harris, K. D. M.; Harris, R. K.; Carss, S. A.; Olivieri, A. C. *J. Chem. Soc., Faraday Trans.* **1995**, *91* (18), 3167−3176.

(34) Alarcón, S. H.; Olivieri, A. C.; Carss, S. A.; Harris, R. K. *Magn. Reson. Chem.* **1995**, *33*, 603−606.

(35) Johnson, W. A.; Mehl, R. F. *Am. Inst. Mining Metall. Eng., Inst. Met. Div., Tech. Publ.* **1939**, *1089*, 1−27.

(36) Avrami, M. *J. Chem. Phys.* **1939**, *7*, 1103−1112.

(37) Avrami, M. *J. Chem. Phys.* **1940**, *8*, 212−224.

(38) Avrami, M. *J. Chem. Phys.* **1941**, *9*, 177−184.

(39) Kolmogorov, A. N. *Bull. Acad. Sci. USSR, Phys. Ser.* **1937**, *1*, 355−359.

(40) Abdelmoty, I.; Buchholz, V.; Di, L.; Guo, C.; Kowitz, K.; Enkelmann, V.; Wegner, G.; Foxman, B. M. *Cryst. Growth Des.* **2005**, *5*, 2210−2217.

(41) Chung, C.-M.; Roh, Y.-S.; Cho, S.-Y.; Kim, J.-G. *Chem. Mater.* **2004**, *16*, 3982−3984.

(42) Lendlein, A.; Jiang, H.; Jünger, O.; Langer, R. *Nature* **2005**, *434*, 879−882.

(43) Valim, J.; Kariuki, B. M.; King, J.; Jones, W. *Mol. Cryst. Liq. Cryst.* **1992**, *211*, 271−281.

(44) Ogawa, M.; Kuroda, K. *Chem. Rev.* **1995**, *95*, 399−438.